frontiers | Frontiers in Chemical Biology

TYPE Original Research
PUBLISHED 06 September 2024
DOI 10.3389/fchbi.2024.1444359

OPEN ACCESS

EDITED BY
Isabel Correia,
University of Lisbon, Portugal

REVIEWED BY
Salete S. Balula,
Chemistry and Technology Network (REQUIMTE), Portugal
Rami Oweini,
University of La Verne, United States

*CORRESPONDENCE
Nadiia I. Gumerova,
nadiia.gumerova@univie.ac.at
Annette Rompel,
annette.rompel@univie.ac.at

RECEIVED 05 June 2024
ACCEPTED 17 July 2024
PUBLISHED 06 September 2024

CITATION
Ždrnja M, Gumerova NI and Rompel A (2024), Exploring polyoxometalate speciation: the interplay of concentration, ionic strength, and buffer composition.
Front. Chem. Biol 3:1444359.
doi: 10.3389/fchbi.2024.1444359

Exploring polyoxometalate speciation: the interplay of concentration, ionic strength, and buffer composition

Maja Ždrnja, Nadiia I. Gumerova* and Annette Rompel*

Universitätä Wien, Fakultät für Chemie, Institute für Biophysikalische Chemie, Wien, Austria

This study investigates the concentration-dependent speciation and stability of Keggin-type $[P^{V}W^{VI}_{12}O_{40}]^{3-}$ **(PW_{12})** and Wells-Dawson type $[\alpha\text{-}P^{V}_{2}W^{VI}_{18}O_{62}]^{6-}$ **(P_2W_{18})** polyoxotungstates across the pH range from two to eight and buffer systems including acetic acid-sodium acetate, citric acid-sodium citrate, sodium phosphate, Tris-HCl and HEPES. Utilizing ^{31}P Nuclear Magnetic Resonance spectroscopy for detailed analysis, we quantified the stability and hydrolysis patterns of **PW_{12}** and **P_2W_{18}** in various buffer solutions at concentrations of 3, and 15 mM, and compared with previously published data for 10 mM solutions. Our research shows that higher concentrations of **PW_{12}** and **P_2W_{18}** in solutions improve their stability in neutral to moderately alkaline environments (pH seven and above), making them less prone to hydrolysis. This pronounced effect underscores the crucial role of concentration in optimizing the behavior of polyoxometalates under varying pH levels, revealing a strong link between concentration and stability across various buffers and highlighting how ionic strength, buffer composition, and pH crucially interact to influence POM stability. Research on how ionic strength affects the speciation of 3 mM solutions shows that the stability of **P_2W_{18}** decreases as the pH approaches neutrality and as ionic strength increases, indicating heightened hydrolysis and reduced stability. For the inherently less stable **PW_{12}**, the findings indicate a shift in hydrolysis pathways—different concentrations of the hydrolysis products, a change likely driven by the increased ionic strength. These findings emphatically underscore the critical importance of meticulously selecting the right buffer and concentration to fully unlock the potential of polyoxometalates such as **PW_{12}** and **P_2W_{18}**. Strategic choices are essential for leveraging these compounds as pivotal elements in groundbreaking applications, poised to revolutionize scientific and technological landscapes.

KEYWORDS

polyoxotungstate, Keggin-type anion, Wells-Dawson-type anion, ionic strength, metal-oxides

1 Introduction

Polyoxometalates (POMs) are versatile, predominantly anionic metal-oxide clusters that have garnered significant attention due to their diverse structures and solubility in aqueous solutions (Pope, 1983; Pope and Müller, 1991). These properties render POMs particularly useful in a variety of applications, ranging from homogeneous catalysis (Kozhevnikov, 1998; Wang and Yang, 2015; Blasco-Ahicart et al., 2018) to roles as

10.3389/fchbi.2024.1444359

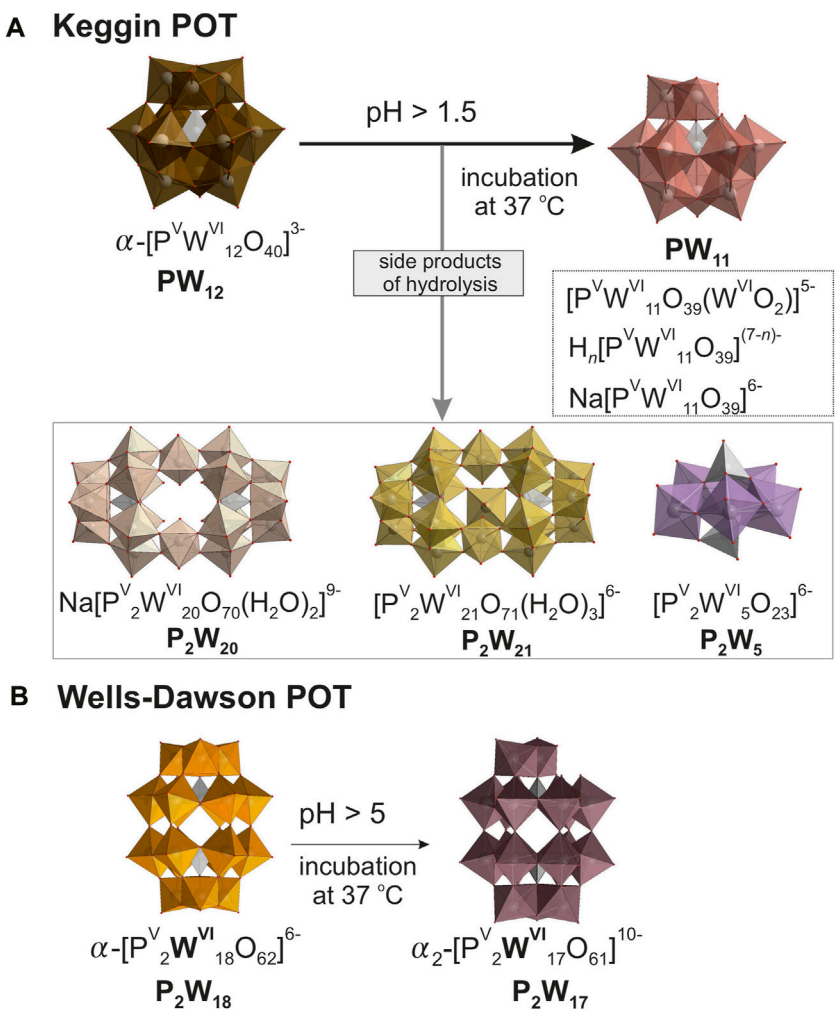

FIGURE 1
Structures and hydrolysis schematics for 10 mM solutions of investigated compounds. Depicted are the molecular structures of **(A)** Keggin type [α $P^{V}W^{VI}_{12}O_{40}]^{3-}$ (**PW_{12}**) and **(B)** Wells-Dawson type [α-$P^{V}_{2}W^{VI}_{18}O_{62}]^{6-}$ (**P_2W_{18}**) polyoxotungstetes (POTs), accompanied by simplified schematics of their hydrolysis pathways. Color code: (WO_6), brown, pink, beige, yellow, lavender, orange, and taupe; (PO_4), grey; O, red. *n* for $H_n[P^{V}W^{VI}_{11}O_{39}]^{(7-n)-}$ is between 0 and 4. To identify the individual anions, they are shown in different colors, with the same color code being selected for a specific anion throughout all Figures and Tables in the main manuscript and the Supplementary Material.

biologically active agents (Bijelic et al., 2018; Bijelic et al., 2019; Aureliano et al., 2021a; Aureliano et al., 2021b; Gumerova and Rompel, 2021). In solution, POMs exhibit a complex behavior including protonation, hydrolysis, and redox reactions, which significantly affect their stability and function (Gumerova and Rompel, 2020). Understanding these behaviors is crucial for harnessing their full potential in practical applications.

To systematically study and document the speciation of POMs—i.e., the composition, concentration, and oxidation states of POMs under various conditions—we previously developed a speciation atlas (Gumerova and Rompel, 2023). This atlas serves as both a comprehensive database and a predictive model for the behavior of POMs in aqueous solutions, facilitating the exploration of their roles in catalysis and biology. The atlas, mainly based on extensive Nuclear Magnetic Resonance (NMR) spectroscopic analysis, has revealed previously unknown behaviors of these compounds, highlighting the intricate nature of their stability and reactivity in solution. Despite these advancements, the concentration-dependent behavior of specific POMs remains insufficiently explored. Our prior work established a foundational understanding of ten polyoxometalates, including Keggin-type $[P^{V}W^{VI}_{12}O_{40}]^{3-}$ (**PW_{12}**) (Keggin, 1933) and Wells-Dawson type [α-$P^{V}_{2}W^{VI}_{18}O_{62}]^{6-}$ (**P_2W_{18}**) (Graham and Finke, 2008) (Figure 1), under standard concentration of 10 mM typically employed in catalytic and biological studies for stock solutions. However, the impact of varying these concentrations on POM speciation and resultant functionalities has not been fully delineated, indicating a clear need for further investigation.

The selection of **PW_{12}** and **P_2W_{18}** for this study is driven by their broad representation in research and their proven efficacy across a spectrum of practical applications. **PW_{12}** has demonstrated a high efficiency and selectivity as an adsorbent for removing antibiotics and heavy metals from water, showcasing its potential in environmental remediation efforts (Zhang et al., 2022). Beyond environmental applications, **PW_{12}** has also shown promising results in medical research. It has been explored as a potential preventative

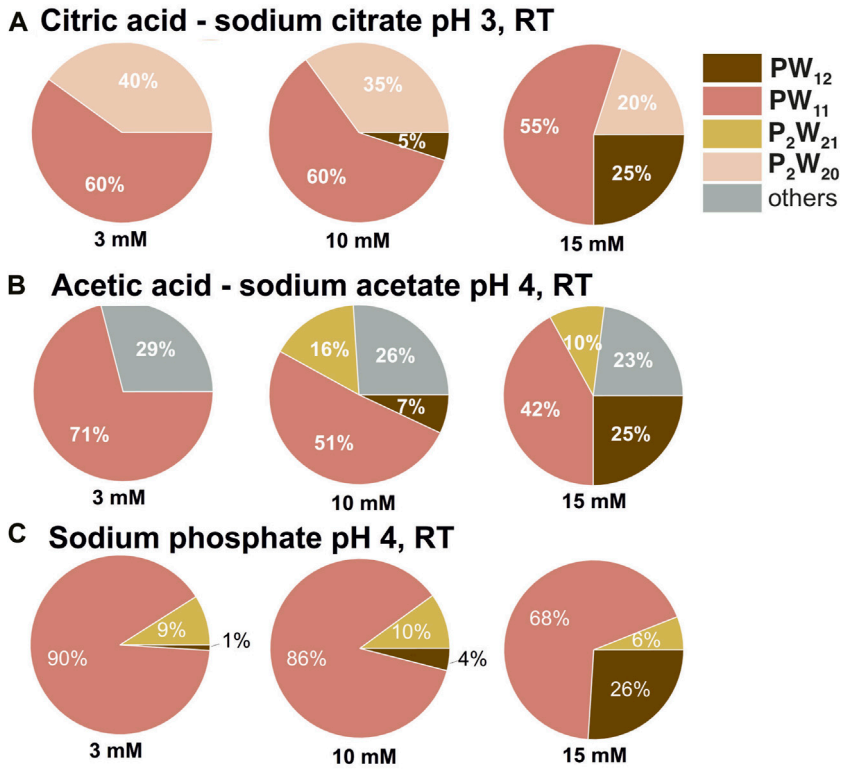

FIGURE 2
Speciation in PW_{12} solutions at pH three and four. Pie chart showing percentages of P-containing POT species in 3, 10, and 15 mM solutions of **PW_{12}** in 0.1 M buffers at pH 3 **(A)** and 4 **(B,C)**. POT concentration values are given as mean values; standard deviations are given in Supplementary Tables S5–S8. Data for 10 mM solutions is taken from (Gumerova and Rompel, 2023).

and therapeutic agent for inflammatory bowel disease (Wang et al., 2021) and exhibits notable anti-cancer effects, particularly against glioblastoma cells (Petronek et al., 2022), highlighting its potential in pharmacological contexts. Similarly, **P_2W_{18}** has been identified for its robust anti-quorum sensing, antibiofilm, and antiviral activities, which are essential for advancing antimicrobial strategies (Faleiro et al., 2022). Moreover, it has been noted for inhibiting aquaporin-3 activity and demonstrating significant anti-cancer activity against human melanoma, further underscoring its utility in therapeutic applications (Pimpao et al., 2020).

Our research reveals insights into the speciation of **PW_{12}** and **P_2W_{18}** in buffered solutions with their concentrations of 10 mM (Gumerova and Rompel, 2023). In acidic conditions, the Keggin-type **PW_{12}** anion shows notable instability, quickly transitioning to its monolacunary form $[P^{V}W^{VI}_{11}O_{39}]^{7-}$ (**PW_{11}**, Figure 1A), upon dissolution in all studied buffers. Interestingly, while incubation generally does not alter speciation dynamics in more stable environments like acetic acid–sodium acetate, it significantly increases the prevalence of hydrolysis products in less stable settings such as sodium phosphate. Under neutral conditions, **PW_{12}** is largely absent, except for minor traces in specific buffers like Tris-HCl. The speciation changes dramatically as the pH moves toward alkalinity, where **PW_{12}** disappears entirely, and **PW_{11}** is formed alongside other hydrolysis products (Figure 1A), reflecting a clear trend towards increased hydrolysis with rising pH levels. The Wells-Dawson **P_2W_{18}** anion (Figure 1B) in 10 mM solution displays robust stability, maintaining nearly 100% integrity across various buffers between pH three and five even after 24 h incubation at 37°C. However, as pH increases to 5.5 and above, significant hydrolysis begins; for example, in acetic acid–sodium acetate and sodium phosphate at pH 6, approximately 20%–35% of **P_2W_{18}** converts into its monolacunary form $[P^{V}_{2}W^{VI}_{17}O_{61}]^{6-}$ (**P_2W_{17}**, Figure 1B), and by pH 8, complete hydrolysis occurs. Collectively, these observations highlight that the stability and speciation of **PW_{12}** and **P_2W_{18}** are profoundly affected by pH and buffer composition, with notable significant hydrolysis in neutral to basic conditions.

In more concentrated solutions, POMs tend to exhibit increased stability due to phenomena such as aggregation and enhanced electrostatic interactions. POMs aggregate more in concentrated solutions, leading to decreased electrostatic repulsion and increased overall stability (Pigga and Liu, 2010). Such aggregation reduces the effective surface area exposed to destabilizing interactions, while the close association of counter-ions around macroions in these solutions diminishes the net charge on the macroions. Furthermore, molecular dynamics simulations have shown that the type and concentration of counterions can significantly influence the degree of ion aggregation and the dynamic properties of POMs, particularly in concentrated solutions (Chaumont and Wipff, 2008).

Ionic strength, a fundamental parameter in solution chemistry, is defined as half the sum of the concentration (c_i) of each ion with the square of its charge (z_i) (Equation 1) (Beyon and Easterby, 1996):

$$I = \frac{1}{2}\sum_{i=1}^{n}\left(c_i \cdot z_i^2\right) \quad (1)$$

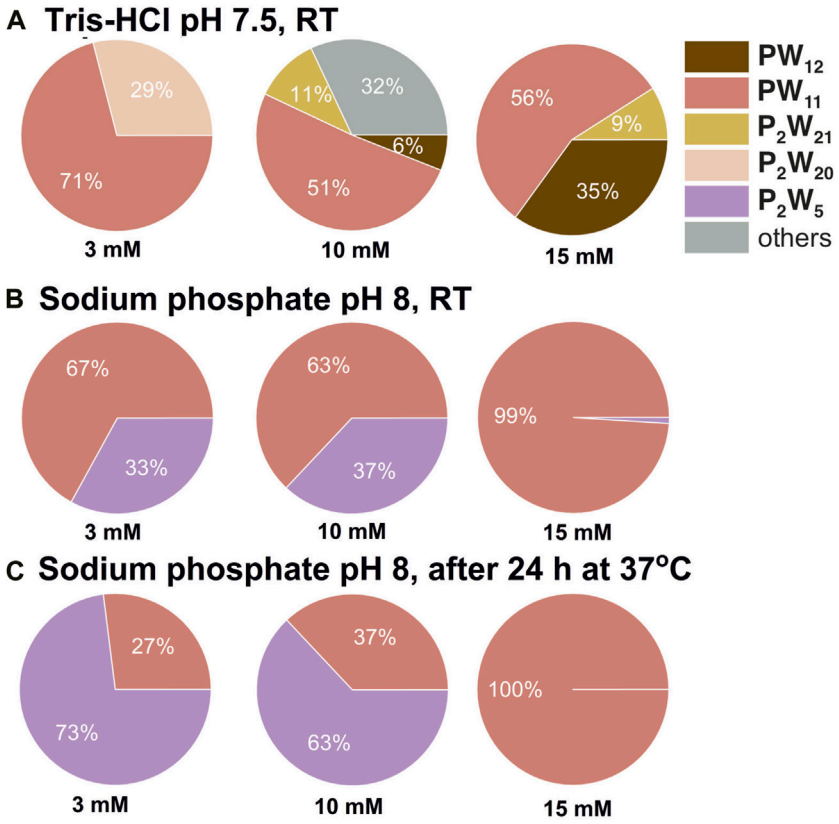

FIGURE 3
Speciation in PW_{12} solutions at pH 7.5 and 8. Pie chart showing percentages of P-containing POT species in 3, 10, and 15 mM solutions of $\mathbf{PW_{12}}$ in 0.1 M buffers at pH 7.5 **(A)** and 8 **(B,C)**. POT concentration values are given as mean values; standard deviations are given in Supplementary Tables S5–S8. Data for 10 mM solutions is taken from (Gumerova and Rompel, 2023).

This measure critically influences the physical and chemical properties of solutions, impacting interactions such as protonation, conformation, and aggregation. Research has consistently highlighted the significant role of ionic strength in various chemical and biological systems. For instance, molecular dynamics simulations demonstrated the importance of ionic strength in coupling protonation and conformational changes in biomolecules (Machuqueiro and Baptista, 2006). In the realm of inorganic chemistry, Casas et al. (2000) used an ion-association equilibrium model to illustrate how ionic strength influences the speciation of ions in sulfuric acid–cupric sulfate solutions. Furthermore, it was found that ionic strength impacted the structure and dynamics of sodium poly(styrensulfonate) solutions, influencing the formation of large multichain domains (Sedlák, 1996).

The role of ionic strength in the speciation and stability of POMs in solution presents another layer of complexity that warrants detailed exploration. Research in this area has revealed that ionic strength not only affects the stability and structural transformations of POMs but also influences their functional behavior (Gumerova and Rompel, 2020). The influence of ionic strength extends to the phase transitions of POMs, as shown by (Thomas et al., 2018). Their study observed that both temperature and ionic strength are critical in driving the transitions of POMs from true solutions to colloidal softoxometalates (SOMs) — larger structures characterized by supramolecular interactions and soft-matter properties—and eventually to crystalline forms (Thomas et al., 2018). This transition underscores the role of ionic strength in stabilizing colloidal phases, which could be crucial for applications that leverage the unique properties of colloids. The interaction of POMs with biological molecules also underscores the significance of ionic strength. For instance, the increasing ionic strength reduces the binding constant of POMs to human serum albumin (Zhang et al., 2007). This finding suggests that the interactions between POMs and proteins are predominantly electrostatic, pointing to the potential modulation of POM bioactivity through manipulation of ionic strength.

In this study, we aim to expand on our existing speciation atlas (Gumerova and Rompel, 2023) by exploring additional concentrations of the Keggin-type $\mathbf{PW_{12}}$ and the Wells-Dawson-type $\mathbf{P_2W_{18}}$. We specifically focused on two concentrations, 3 mM and 15 mM, by expanding the concentration range beyond the previously studied 10 mM (Gumerova and Rompel, 2023), we aimed to provide a broader understanding of their behavior under varying conditions. This approach allowed us to observe how changes in concentration influence the stability and interactions of these compounds, enabling a more comprehensive comparison and analysis against the existing data.

2 Materials and methods

All chemicals were purchased from Sigma-Aldrich (Austria) and used without further purification.

TABLE 1 Overview of selected buffers, temperatures, concentrations, and ionic strengths for stability studies on Keggin and Wells-Dawson polyoxotungstates (POTs).

pH range	Buffer type	Temperature (°C)	Concentration (mM)	Ionic strength	Number of conditions
Strongly acidic environment **2 ≤ pH ≤ 4**	1) 0.1 M Sodium phosphate pH 2, 3, 4; 2) 0.1 M citric acid—sodium citrate pH 3, 4; 3) 0.1 M acetic acid—sodium acetate pH 4	RT and 24 h incubation at 37	3; 15	0.1 M Sodium phosphate at pH 4 was additionally tested wih three concentrations: 100 mM, 200 mM, and 300 mM of $NaNO_3$	30
Moderately acidic environment **5 ≤ pH ≤ 6**	1) 0.1 M Sodium phosphate pH 5, 6; 2) 0.1 M citric acid—sodium citrate pH 5, 6; 3) 0.1 M acetic acid—sodium acetate pH 5, 5.5	RT and 24 h incubation at 37	3; 15	–	24
Neutral environment **6.5 ≤ pH ≤ 7.5**	1) 0.1 M citric acid—sodium citrate pH 6.5; 2) 0.1 M Sodium phosphate pH 7; 3) 0.1 M HEPES pH 7, 7.5; 4) 0.1 M Tris-HCl pH 7, 7.5	RT and 24 h incubation at 37	3; 15	0.1 M Sodium phosphate pH 7 was additionally tested wih three concentrations: 100 mM, 200 mM, and 300 mM of $NaNO_3$	30
Moderately alkaline environment **pH = 8**	1) 0.1 M Sodium phosphate pH 8; 2) 0.1 M HEPES pH 8; 3) 0.1 M Tris-HCl pH 8	RT and 24 h incubation at 37	3; 15	0.1 M HEPES pH 8 and 0.1 M Tris-HCl pH 8 were additionally tested wih three concentrations: 100 mM, 200 mM, and 300 mM of $NaNO_3$	24
In total for one POT conditions (each was measured in triplicate)					**Σ108** (324 spectra for each POT were collected)

2.1 Buffer characteristics and preparation

Buffer solutions exhibit an optimal pH range wherein they exhibit maximal efficacy in moderating changes in hydrogen ion concentration while preserving pH stability. This range is primarily delineated by the acid dissociation constant (K_a) of the buffer compound and is conventionally defined as the pK_a (–logK_a) value with an allowance of plus or minus one pH unit (Beyon and Easterby, 1996). For the study of polyoxometalates in solution, we used five different buffers covering a pH range from two to eight. In the acidic range, three anionic buffers—acetic acid-sodium acetate buffer NaOAC/HOAc [pH 4–5.5, pK_a = 4.76 (Harned, 1958)], citric acid-sodium citrate Na_3Cit/H_3Cit [pH 3–6.5, pK_a = 3.13, 4.76, 6.40 (Harned, 1958)] and sodium phosphate buffer NaH_2PO_4/H_3PO_4, Na_2HPO_4/NaH_2PO_4 (pH 2—6, pK_a = 2.15, 6.86 (Harned, 1958); while phosphate does not buffer in the pH range of 3.5—5.5, experiments were conducted at this pH to provide comparisons to previously published studies (Collins-Wildman et al., 2018). In the neutral and basic medium, two ionic: sodium phosphate Na_2HPO_4/NaH_2PO_4 [pH 7—8, pK_a = 6.86 (Harned, 1958)], and Tris-HCl (pH 7—8, pK_a = 8.06 [(Harned, 1958), Supplementary Figure S1], and one zwitterionic buffer: HEPES [4-(2-hydroxyethyl)-1-piperazineethanesulfonic acid, pH 7—8, pK_a = 7.5 (Good et al., 1966), Supplementary Figure S1] have been studied. All buffers were prepared at a concentration of 0.1 M using the Henderson-Hasselbalch (Po and Senozan, 2001) Equation 2:

$$\mathrm{pH} = \mathrm{p}K_a + \log_{10}\left(\left[\text{proton acceptor}\right]/\left[\text{proton donor}\right]\right) \quad (2)$$

The influence of ionic strength was assessed using several anionic buffers: anionic buffers—acetic acid-sodium acetate buffer NaOAC/HOAc pH 4 [pK_a = 4.76 (Harned, 1958)], sodium phosphate Na_2HPO_4/NaH_2PO_4 [pH 7, pK_a = 6.86 (Harned, 1958)], Tris-HCl [pH 7, pK_a = 8.06 (Harned, 1958)]; and one zwitterionic buffer HEPES pH 7 [pK_a = 7.5 (Good et al., 1966)]. Each buffer was supplemented with the strong electrolyte $NaNO_3$ at concentrations of 100 mM, 200 mM, and 300 mM.

2.2 POM synthesis and characterization

Keggin-type $Na_3[P^{V}W^{VI}{}_{12}O_{40}]\cdot 8.5H_2O$ (CAS-Number: 312,696–30-3, $\mathbf{PW_{12}}$) was purchased from Merck (Austria) as the commercially available compounds are commonly used in applications. Wells-Dawson type $K_6[\alpha\text{-}P^{V}{}_2W^{VI}{}_{18}O_{62}]\cdot 14H_2O$ ($\mathbf{P_2W_{18}}$) was synthesized according to the published procedure (Graham and Finke, 2008). Both POTs were characterized in solid-state using infrared (IR) spectroscopy (Supplementary

10.3389/fchbi.2024.1444359

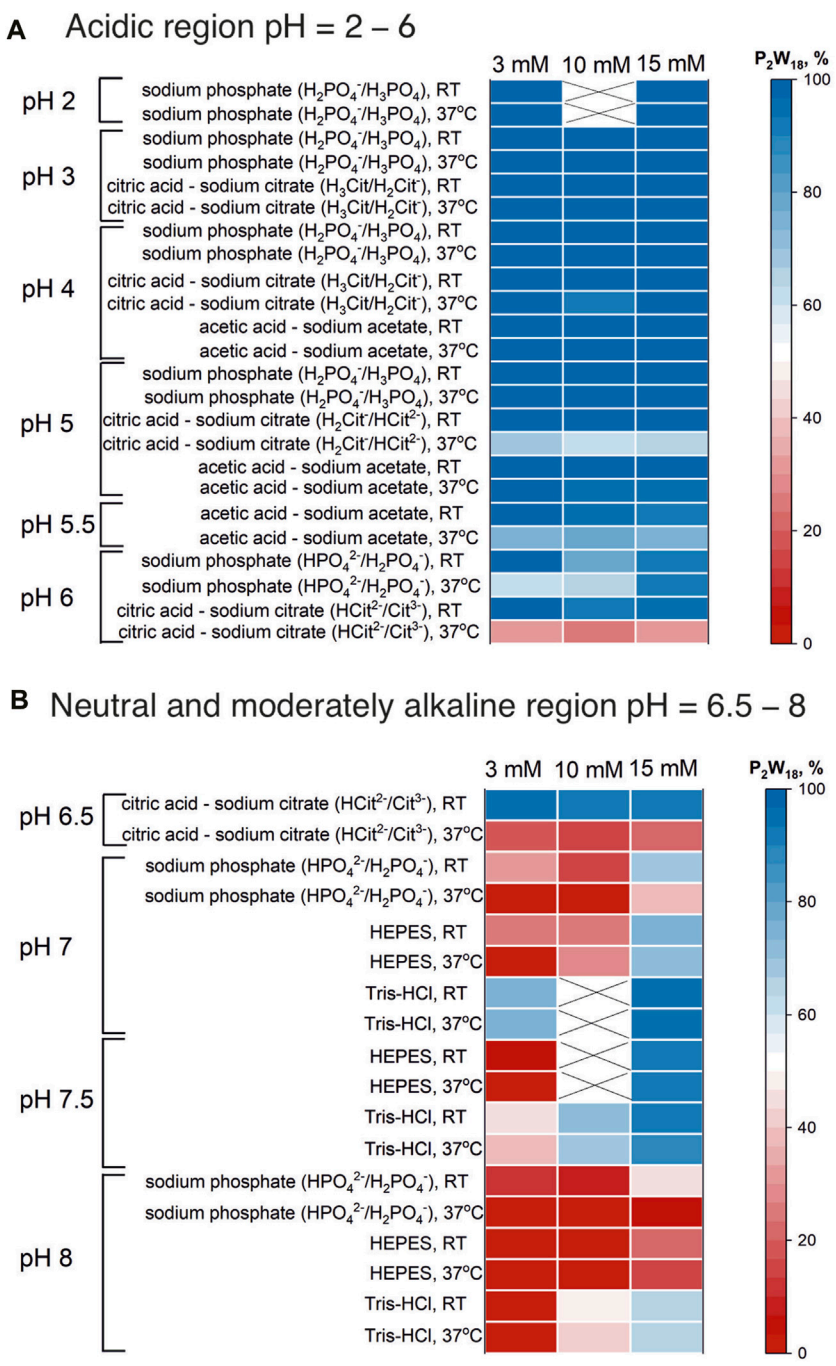

FIGURE 4
"Heat map" of $\mathbf{P_2W_{18}}$ stability in acidic **(A)** and neutral and moderately alkaline **(B)** regions. The "heat map" shows the percentage of the initial anion present in solution at room temperature and after 24 h incubation at 37°C. The map was created on the basis of the integrated data from ^{31}P NMR spectra (see SI). Data for 10 mM solutions is taken from (Gumerova and Rompel, 2023).

Figures S2, S3, Supplementary Table S1), thermogravimetric analysis (TGA, Supplementary Figure S4, Supplementary Table S2), unit cell determination by single crystal X-ray diffraction, and in solution by ^{31}P NMR spectroscopy (Supplementary Figure S5). The determined unit cells for $\mathbf{PW_{12}}$: a = 14.1 Å, b = 14.1 Å, c = 14.0 Å, α = 93°, β = 113°, γ = 118° (ICSD match 4.159); for $\mathbf{P_2W_{18}}$: a = 12.9 Å, b = 14.9 Å, c = 22.3 Å, α = 94°, β = 117°, γ = 115° (ICSD match 24.673).

2.3 Speciation studies

POT solutions were tested with concentrations of 3 mM and 15 mM. Measurements were recorded both initially and after a 24 h incubation at 37°C using a setup that included 10% of deuterium oxide alongside the buffer. Each buffer solution was maintained at a consistent concentration of 0.1 M pH levels were accurately

10.3389/fchbi.2024.1444359

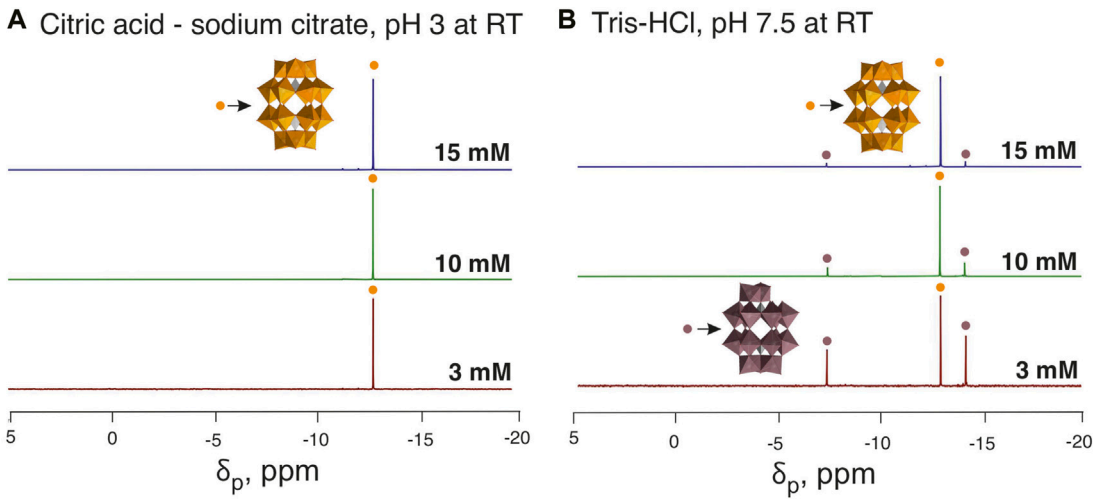

FIGURE 5
^{31}P NMR spectra of buffered P_2W_{18} solutions. Panel **(A)** displays the spectra of $\mathbf{P_2W_{18}}$ in an acidic environment (citric acid—sodium citrate pH 3), showing a consistent signal at −13.1 ppm, which indicates the stability of the Wells-Dawson anion (Massart et al., 1977). Panel **(B)** illustrates spectra in a neutral environment (Tris-HCl pH 7.5), highlighting an increased hydrolysis rate and the formation of $[P^{V}_{2}W^{VI}_{17}O_{61}]^{10-}$ ($\mathbf{P_2W_{17}}$), with signals at −7.3 and −14.1 ppm (Massart et al., 1977), in solutions with the decreased starting concentration of $\mathbf{P_2W_{18}}$. Color code: (WO_6), orange, and taupe; (PO_4), grey; O, red. To identify the individual anions, they are shown in different colors, with the same color code being selected for a specific anion throughout all Figures and Tables in the main manuscript and the Supplementary Material. Data for 10 mM solutions is taken from (Gumerova and Rompel, 2023).

measured using a Thermo Fisher Orion Star A211 benchtop pH meter, which was equipped with a Hamilton Biotrod electrode. Calibration of the electrode was performed before each measurement series using Sigma-Aldrich standard buffers at pH levels of 2.00 (citric acid/sodium hydroxide/hydrogen chloride), 4.01 (potassium hydrogen phthalate), and 7.00 (disodium hydrogen phosphate/potassium dihydrogen phosphate).

Speciation analysis for both the Keggin-type $\mathbf{PW_{12}}$ and the Wells-Dawson-type $\mathbf{P_2W_{18}}$ was performed using ^{31}P NMR spectroscopy. This method allowed for the quantification of the relative abundance of various species by integrating the ^{31}P NMR peaks. The analysis was strictly focused on signals related to POM species, intentionally excluding signals from free phosphate. The ^{31}P NMR spectra were obtained using a Bruker Avance Neo 500-MHz FT-NMR spectrometer at 25°C, with chemical shifts referenced to 85% H_3PO_4. The acquisition frequency was 202.53 MHz, and each experimental session lasted about 15 min. Data processing was conducted using MestraNova software.

3 Results and discussion

3.1 Experimental setup

To study the concentration effect on POMs speciation, the same pH range as in the POM speciation atlas (Gumerova and Rompel, 2023) has been studied, employing buffer types under conditions previously used in catalytic and biological applications. The range from pH two to eight is generally covered using anionic buffers (acetic acid–sodium acetate, citric acid–sodium citrate, sodium phosphate, and Tris-HCl, along with organic Good's buffers such as HEPES, MES, and glycine-NaOH (Good et al., 1966). From our previous studies (Gumerova and Rompel, 2023), we found that MES and glycine-NaOH did not maintain the desired pH stability in POM systems and therefore have been excluded from the current study. For this study, we did not utilize complex media like Mueller-Hinton broth (MHB) or nutrient mixture F-12 Ham, which were previously employed. The uncertain buffering capacity of these media could obscure the effects of concentration changes, potentially leading to unreliable data regarding the desired speciation dynamics. In our current experiments, higher POM concentrations of 15 mM were challenging to dissolve in MHB and F-12-Ham due to their complex composition, and lower concentrations of 3 mM did not yield sufficiently strong NMR signals for reliable speciation analysis due to already present free phosphate in these media that suppressed POM signals. Instead, we focused on optimizing buffer conditions to enhance comparison and data reliability. Specifically, we standardized the use of Tris-HCl and HEPES buffers at pH values of 7, 7.5, and 8. These pH settings were chosen to facilitate a better comparison between two of the most common buffers used in biological applications—one of anionic nature and the other zwitterionic. To complete the pH range coverage in phosphate buffers, we included a highly acidic sodium phosphate buffer at pH 2. In all tested buffered solutions, the solubility of both POTs was sufficient to get clear solutions even after 24 h of incubation.

POM investigations are usually performed at room temperature, so initially, all speciation measurements were done under standard conditions [1 atm (101,325 Pa), 25°C (298 K)]. To investigate the influence of temperature on POMs' speciation, all solutions measured at room temperature were subsequently incubated at 37°C for 24 h and measured again. This takes the physiological temperature into account and gives the first insights into the speciation of POMs at temperatures above room temperature.

10.3389/fchbi.2024.1444359

TABLE 2 The concentration of the intact $[P^{V}_{2}W^{VI}_{18}O_{62}]^{6-}$ anion in POM solutions at three different concentrations (3, 10, and 15 mM) dissolved in acetic acid—sodium acetate pH 4—5.5; sodium phosphate pH 2—8 [while phosphate does not buffer at pH range from 3.5—5.5, experiments were conducted at this pH to provide comparisons to previously published studies (Collins-Wildman et al., 2018)]; citric acid—sodium citrate pH 3—6.5; Tris-HCl pH 7—8; HEPES pH 7—8; with concentration of 0.1 M. The species content was calculated based on the integration of ^{31}P signals considering only signals associated with POTs. Signals were assigned based on the literature data (Gumerova and Rompel, 2023). Detailed speciation data are summarized in Supplementary Tables S11–S14.

Buffer	% of P_2W_{18} (mean ± SD[a]) at RT in K_6 [α-$P^{V}_{2}W^{VI}_{18}O_{62}$] solution at concentrations of			% of P_2W_{18} (mean ± SD[a]) in K_6 [α-$P^{V}_{2}W^{VI}_{18}O_{62}$] solution after 24 h incubation at 37°C solution at concentrations		
	3 mM	10 mM[b]	15 mM	3 mM	10 mM[b]	15 mM
Strong[b] acidic environment 2 ≤ pH ≤ 4						
0.1 M Sodium phosphate ($H_2PO_4^-/H_3PO_4$) pH 2	100 ± 0	–	100 ± 0	100 ± 0	–	100 ± 0
0.1 M Sodium phosphate ($H_2PO_4^-/H_3PO_4$) pH 3	100 ± 0	100 ± 0	100 ± 0	100 ± 0	100 ± 0	100 ± 0
0.1 M Citric acid—sodium citrate (H_3Cit/H_2Cit^-) pH 3	100 ± 0	100 ± 1	100 ± 0	100 ± 0	100 ± 0	100 ± 0
0.1 M Sodium phosphate ($H_2PO_4^-/H_3PO_4$) pH 4	100 ± 0	100 ± 0	100 ± 0	100 ± 0	100 ± 0	100 ± 0
0.1 M Citric acid—sodium citrate ($H_2Cit^-/HCit^{2-}$) pH 4[c]	100 ± 0	100 ± 1	100 ± 0	98 ± 1	[c]3 ± 6	98 ± 0
0.1 M acetic acid—sodium acetate (OAc^-/HOAc) pH 4	100 ± 0	100 ± 0	100 ± 0	100 ± 0	100 ± 0	100 ± 0
Moderately acidic environment 5 ≤ pH ≤ 6						
0.1 M Sodium phosphate ($H_2PO_4^-/H_3PO_4$) pH 5	100 ± 0	99 ± 0	100 ± 0	100 ± 0	99 ± 0	100 ± 0
0.1 M Citric acid—sodium citrate ($H_2Cit^-/HCit^{2-}$) pH 5[c]	100 ± 0	98 ± 2	98 ± 0	69 ± 0	62[c] ± 4	64 ± 3
0.1 M acetic acid—sodium acetate (OAc^-/HOAc) pH 5	100 ± 0	98 ± 1	97 ± 1	98 ± 0	95 ± 2	95 ± 0
0.1 M Sodium phosphate ($HPO_4^{2-}/H_2PO_4^-$) pH 6	98 ± 0	78 ± 3	93 ± 0	60 ± 2	65 ± 3	92 ± 0
0.1 M Citric acid—sodium citrate ($HCit^{2-}/Cit^{3-}$) pH 6[c]	98 ± 2	91 ± 5	94 ± 1	31 ± 1	24[c] ± 6	31± 1
Neutral environment 6.5 ≤ pH ≤ 7.5						
0.1 M Citric acid—sodium citrate ($HCit^{2-}/Cit^{3-}$) pH 6.5[c]	96 ± 4	90 ± 3	92 ± 0	19 ± 1	15[c] ± 5	22 ± 1
0.1 M Sodium phosphate ($HPO_4^{2-}/H_2PO_4^-$) pH 7	30 ± 1	14 ± 3	67 ± 2	0	0	39 ± 1
0.1 M HEPES[d] pH 7	26 ± 4	35 ± 4	75 ± 1	2 ± 2	29 ± 1	73 ± 0
0.1 M Tris-HCl[e] pH 7	75 ± 1	–	95 ± 0	76 ± 2	–	9[e] ± 0
0.1 M HEPES[d] pH 7.5	5 ± 2	–	90 ± 1	0	–	93 ± 6
0.1 M Tris-HCl[e] pH 7.5	44 ± 2	70 ± 5	90 ± 0	39[e] ± 1	69 ± 6	89 ± 1
Moderately alkaline environment pH = 8						
0.1 M Sodium phosphate ($HPO_4^{2-}/H_2PO_4^-$) pH 8	11 ± 2	9 ± 3	46 ± 1	0	0	6 ± 1
0.1 M HEPES[d] pH 8	0	0	21 ± 1	0	0	14 ± 1
0.1 [d] Tris-HCl[e] pH 8	0	48 ± 9	66 ± 3	0	42 ± 2	6[e] ± 3

[a]SD, standard deviation.

[b]Data i[a] taken from (Gumerova and[b]Rompel, 2023).

[c]Note, The integration of.

[31]P NM[c], spectra is a complex task, and the reported concentrations of species may exhibit variability. However, these values are considered acceptable within the standard deviation (SD) range. All measurements were performed in triplicate to ensure consistency and reliability of the data.

[d]HEPES, 4-(2-hydroxyethyl)-1-piperazineethanesulfonic acid, $C_8H_{18}N_2O_4S$ (Supplementary Figure S1).

[e]Tris—Tris (hydroxymethyl)aminom[e]thane, $C_4H_{11}NO_3$ (Supplementary Figure S1).

3.2 Concentration-dependent speciation of PW_{12}

The Keggin POT **PW_{12}** exhibits a remarkable sensitivity towards hydrolysis, demonstrating limited stability even under strongly acidic conditions (Maksimovskaya and Maksimov, 2019; Gumerova and Rompel, 2023). Increasing the concentration of **PW_{12}** in solution does not improve its overall stability (Supplementary Tables S5–S8). For example, in sodium acetate–acetic acid buffer solutions at pH four at a concentration of 3 mM, **PW_{12}** is notably absent from the solution entirely (Figure 2A). As the concentration of **PW_{12}** is increased to

10.3389/fchbi.2024.1444359

TABLE 3 The concentration of the intact $[P^V_2W^{VI}_{18}O_{62}]^{6-}$ anion in P_2W_{18} solutions (3 mM) dissolved in acetic acid—sodium acetate pH 4, sodium phosphate pH 7, Tris-HCl pH 8, and HEPES pH 8 with concentration of 0.1 M. Each buffer was tested both without the addition of $NaNO_3$ and with $NaNO_3$ added at three different concentrations: 100 mM, 200 mM, and 300 mM. The species content was calculated based on the integration of ^{31}P signals considering only signals associated with POTs. Signals were assigned based on the literature data (Gumerova and Rompel, 2023). Detailed speciation data are summarized in Supplementary Tables S17, S18.

Buffer	% Of P_2W_{18} at RT in K_6 [α-$P^V_2W^{VI}_{18}O_{62}$] (3 mM) solution at concentrations of $NaNO_3$				% Of P_2W_{18} in K_6 [α-$P^V_2W^{VI}_{18}O_{62}$] (3 mM) solution after 24 h incubation at 37°C solutions at concentrations of $NaNO_3$			
	0 mM	100 mM	200 mM	300 mM	0 mM	100 mM	200 mM	300 mM
0.1 M acetic acid—sodium acetate (OAc^-/HOAc) pH 4	100 ± 0	100 ± 0	100 ± 0	100 ± 0	100 ± 0	100 ± 0	100 ± 0	100 ± 0
0.1 M sodium phosphate (HPO_4^{2-}/$H_2PO_4^-$) pH 7	30 ± 1	44 ± 2	13 ± 2	6 ± 1	0	0	0	0
0.1 M HEPES pH 8	0	0	0	0	0	0	0	0
0.1 M Tris-HCl pH 8	0	0	0	0	0	0	0	0

TABLE 4 The concentration of the main hydrolysis products $[P^VW^{VI}_{11}O_{39}]^{7-}$ (PW_{11}) and $[P^V_2W^{VI}_5O_{23}]^{6-}$ (P_2W_5) anions in P_2W_{18} solutions (3 mM) dissolved in acetic acid—sodium acetate pH 4, sodium phosphate pH 7, Tris-HCl pH 8, and HEPES pH 8 with concentration of 0.1 M. Each buffer was tested both without the addition of $NaNO_3$ and with $NaNO_3$ added at three different concentrations: 100 mM, 200 mM, and 300 mM. The species content was calculated based on the integration of ^{31}P signals considering only signals associated with POTs. Signals were assigned based on the literature data (Gumerova and Rompel, 2023). Detailed speciation data are summarized in Supplementary Tables S19, S20.

Buffer	% Of PW_{11} at RT in Na_3 [$P^VW^{VI}_{12}O_{40}$] (3 mM) solutions with concentrations of $NaNO_3$				% Of PW_{11} in Na_3 [$P^VW^{VI}_{12}O_{40}$] (3 mM) solutions after 24 h incubation at 37°C with concentrations of $NaNO_3$			
	0 mM	100 mM	200 mM	300 mM	0 mM	100 mM	200 mM	300 mM
0.1 M acetic acid—sodium acetate (OAc^-/HOAc) pH 4	68 ± 1	70 ± 2	83 ± 2	76 ± 4	100 ± 0	73 ± 0	91 ± 2	90 ± 2
0.1 M HEPES pH 8	100 ± 0	100 ± 00	100 ± 0	100 ± 0	100 ± 0	100 ± 00	100 ± 0	100 ± 0
0.1 M Tris-HCl pH 8	100 ± 0	49 ± 1	100 ± 0	100 ± 0	100 ± 0	47 ± 0	100 ± 0	100 ± 0
Buffer	**% of PW_{11}/P_2W_5 at RT in $Na_3[P^VW^{VI}_{12}O_{40}]$ (3 mM) solutions with concentrations of $NaNO_3$**				**% of PW_{11}/P_2W_5 at RT in $Na_3[P^VW^{VI}_{12}O_{40}]$ (3 mM) solutions after 24 h incubation at 37°C with concentrations of $NaNO_3$**			
	0 mM	100 mM	200 mM	300 mM	0 mM	100 mM	200 mM	300 mM
0.1 M Sodium phosphate (HPO_4^{2-}/$H_2PO_4^-$) pH 7	67 ± 0/ 33 ± 0	67 ± 0/ 33 ± 0	67 ± 0/ 33 ± 0	67 ± 0/ 33 ± 0	50 ± 0/ 50 ± 0	50 ± 0/ 50 ± 0	23 ± 0/ 77 ± 0	18 ± 1/ 82 ± 1

10 mM and 15 mM, its relative abundance within the solution rises only to 7% and 25%, respectively (Figure 2A). A similar trend of increased $\mathbf{PW_{12}}$ stability is observed in other buffers under strongly acidic conditions −3 < pH < 4 (Figure 2; Supplementary Tables S5–S8). However, this effect is not apparent at pH values above 5. In these higher pH solutions, the concentration of POT only influences the composition of the hydrolysis mixture (Figure 2B).

The higher concentrations of $\mathbf{PW_{12}}$ actually promotes the formation of a more complex mixture of hydrolyzed species, which were identified according to the literature data (Maksimovskaya and Maksimov, 2019). At lower $\mathbf{PW_{12}}$ concentrations, the final hydrolysis product $[P^VW^{VI}_{11}O_{39}]^{7-}$ [$\mathbf{PW_{11}}$, (Contant, 1987)], appears to be the dominant species (Supplementary Tables S5–S8). This can be demonstrated using citric acid—sodium citrate buffer as an example. At a concentration of 3 mM $\mathbf{PW_{12}}$, only $\mathbf{PW_{11}}$ and $[P^V_2W^{VI}_{20}O_{70}(H_2O)_2]^{10-}$ [$\mathbf{P_2W_{20}}$, (Bajpe et al., 2012)] are present in significant quantities throughout the entire investigated pH range (Supplementary Tables S5–S8). However, when the concentration of $\mathbf{PW_{12}}$ is increased to 10 and 15 mM, a wider variety of hydrolysis products become evident, including $[P^V_2W^{VI}_{21}O_{71}(H_2O)_3]^{6-}$ [$\mathbf{P_2W_{21}}$, (Tourné et al., 1986)] and $[P^V_2W^{VI}_5O_{23}]^{6-}$ [$\mathbf{P_2W_5}$, (Lin et al., 2006)]. This observation suggest that higher $\mathbf{PW_{12}}$ concentrations may favor further hydrolysis pathways leading to the formation of these additional species. Another example of a complexity of the speciation in $\mathbf{PW_{12}}$ solution after hydrolysis is the rearrangements of $\mathbf{PW_{11}}$ to $\mathbf{P_2W_5}$ after incubation. ^{31}P NMR data reveals a higher stability of $\mathbf{P_2W_5}$ compared to $\mathbf{PW_{11}}$ in sodium phosphate buffer at pH 8 after incubation for 24 h at 37°C in both 3 mM and 10 mM of $\mathbf{PW_{12}}$ solutions (Figures 3B,C). Only $\mathbf{PW_{11}}$ is observed at a concentration of 15 mM $\mathbf{PW_{12}}$. This suggests that the interplay between $\mathbf{PW_{12}}$ concentration, pH, and buffer composition significantly influences the equilibrium between its hydrolysis products. Further investigations are necessary to elucidate the underlying mechanisms governing this complex interplay.

Finally, data collected in 3 and 15 mM Keggin POT solutions highlight one more time that some buffers, like Tris-HCl, are not the best choice to keep the pH in POM solutions (Supplementary Tables S3, S4; Supplementary Figure S7). Unlike citrate and phosphate buffers, which maintain a pH at least for low concentrated POT solutions, Tris-HCl exhibits a poor buffering capacity, leading to pH drop up to 5 units (Supplementary Figure S7). This poor buffering capacity hinders the maintenance of $\mathbf{PW_{12}}$ integrity and allows for a detectable presence of intact $\mathbf{PW_{12}}$ even at neutral pH values in Tris-HCl buffers (Figure 3A).

3.3 Concentration-dependent speciation of P_2W_{18}

In solutions with 3 mM and 15 mM $\mathbf{P_2W_{18}}$ concentrations, observed trends are similar to 10 mM $\mathbf{P_2W_{18}}$ solutions (Gumerova and Rompel, 2023), although the pH and species concentrations vary (Supplementary Tables S9–S14). The pH of buffered solutions tends to become more acidic than the initial buffer pH after dissolving higher concentrations of $\mathbf{P_2W_{18}}$, particularly in incubated alkaline solutions. The most pronounced pH drop, up to 2.5 units, occurs after dissolving 15 mM of $\mathbf{P_2W_{18}}$ in buffers initially set at pH 8 (Supplementary Figures S8, S9). In contrast, 3 mM $\mathbf{P_2W_{18}}$ solutions cause only insignificant changes to the buffer pH (Supplementary Figures S8, S9).

The analysis of varying concentrations of $\mathbf{P_2W_{18}}$ (3 mM, 10 mM, and 15 mM) on its stability across different pH levels and buffer solutions (Table 2; Figure 4) shows:

1) *In strongly acidic buffers* such as sodium phosphate and citric acid-sodium citrate at pH levels ranging from two to four, $\mathbf{P_2W_{18}}$ displays exceptional stability at all concentrations (3, 10, and 15 mM). The anion remains fully intact (100%) regardless of concentration, even after 24 h at 37°C. This indicates that under strongly acidic conditions, the concentration does not affect the stability of $\mathbf{P_2W_{18}}$ (Figures 4, 5A).
2) *In moderately acidic environment* (pH 5-6) the stability remains relatively high across all concentrations, though it begins to decrease slightly at 15 mM in citric acid-sodium citrate pH 5, where about 2% degradation is observed initially, increasing to 36% after 24 h. This trend is more pronounced at pH 5.5 and 6, where higher concentrations lead to a more significant reduction in stability, especially in sodium phosphate and acetic acid-sodium acetate buffers (Figure 4).
3) As the pH approaches *neutrality*, the impact of higher concentrations becomes more evident. At pH 7, in sodium phosphate the concentration of the intact anion more than triples as the $\mathbf{P_2W_{18}}$ concentration increases from 3 mM to 10 mM, with this effect becoming even more pronounced after incubation. Similar trends are observed in citric acid-sodium citrate and Tris-HCL buffer at pH 7.5, where higher concentrations of $\mathbf{P_2W_{18}}$ are associated with enhanced stability and reduced hydrolysis rates (Figure 4).
4) *In moderately alkaline environment* at pH 8, in buffers like sodium phosphate and HEPES, there is a notable increase in stability as the concentration increases. For instance, in sodium phosphate, the intact anion's stability is only 11% at 3 mM and increases further to 77% at 15 mM initially, with complete degradation post-incubation for 3 mM solutions. This pattern is consistent across all alkaline buffers, where higher concentrations lead to increased stability (Figure 4).

From the analysis, it is clear that while $\mathbf{P_2W_{18}}$ maintains high stability in strongly acidic conditions irrespective of concentration, its stability decreases in more neutral and alkaline environments, however, in solutions with higher concentrations the stability greatly increased, which is in accordance with findings from previous research (Chaumont and Wipff, 2008; Pigga and Liu, 2010). This suggests that higher concentrations of $\mathbf{P_2W_{18}}$ are less susceptible to hydrolysis and decomposition, particularly in less acidic conditions. This concentration-dependent instability highlights the critical interplay between pH, buffer composition, and $\mathbf{P_2W_{18}}$ concentration, emphasizing the need for careful selection of experimental conditions to maintain the integrity of $\mathbf{P_2W_{18}}$ in practical applications.

3.4 Impact of ionic strength on speciation dynamics

In speciation atlas for 10 mM POM solutions (Gumerova and Rompel, 2023), we observed a marked influence of ionic strength on stability and speciation in buffer solutions with different ionic strength. To isolate effects due to ionic strength from the buffer type, here we compare the stability of POMs in the same buffers but with adjusted ionic strength values made by addition of 100, 200, or 300 mM of $NaNO_3$ (Table 3 and 4).

The $\mathbf{P_2W_{18}}$ anion exhibits remarkable stability in acidic buffers, maintaining 100% integrity both immediately and after 24 h, irrespective of the $NaNO_3$ concentration (Table 3; Supplementary Tables S17, S18). This demonstrates a strong resistance to hydrolysis or degradation under acidic conditions. In contrast, no intact $\mathbf{P_2W_{18}}$ is detected in moderately alkaline buffers, indicating complete hydrolysis or degradation under basic conditions, regardless of the $NaNO_3$ concentration (Supplementary Tables S17, S18). Interestingly, the stability of $\mathbf{P_2W_{18}}$ notably decreases in neutral pH buffers; only 32% remains intact without $NaNO_3$, and this number drops to 0% at higher $NaNO_3$ concentrations (Table 3; Supplementary Tables S17, S18). This suggests enhanced hydrolysis or instability as the pH approaches neutrality and with increasing ionic strength. Previous findings have shown that in solutions with higher ionic strength, anions can act as proximal bases, causing a local increase in pH and thus accelerating the decomposition or rearrangement of the species (Collins-Wildman et al., 2018).

For the inherently unstable $\mathbf{PW_{12}}$, we analyze the changes in the speciation of its hydrolysis products. A transformation occurs where the majority of $\mathbf{PW_{12}}$ converts to $\mathbf{PW_{11}}$ upon hydrolysis. In 0.1 M acetic acid—sodium acetate buffer at pH 4, this conversion progresses to full (100%) after 24 h across all three $NaNO_3$ concentrations tested (Table 4; Supplementary Tables S19, S20). The $\mathbf{PW_{11}}$ species exhibits exceptional stability in HEPES buffer at pH 8, maintaining complete integrity both immediately after preparation and following 24 h of incubation at 37°C, across all

tested concentrations of $NaNO_3$ (0 mM, 100 mM, 200 mM, and 300 mM) (Table 4; Supplementary Tables S19, S20). In Tris-HCl buffer at pH 8, $\mathbf{PW_{11}}$ is the predominant species at 0 mM, 200 mM, and 300 mM $NaNO_3$ concentrations both initially and after 24 h (Table 4; Supplementary Tables S19, S20). However, a noticeable decrease in stability occurs at a $NaNO_3$ concentration of 100 mM, where only 49% (the rest is other hydrolysis species, see Supplementary Tables S19, S20) of $\mathbf{PW_{11}}$ remains intact after 24 h. This specific instability suggests a unique ionic interaction at this concentration, significantly affecting the stability of $\mathbf{PW_{11}}$ in Tris-HCL buffer. The restoration of $\mathbf{PW_{11}}$ domination at higher $NaNO_3$ concentrations (200 mM and 300 mM) indicates a complex relationship between ionic strength and speciation dynamics in this buffer. In sodium phosphate buffer pH 7, an initial balance between $\mathbf{PW_{11}}$ and $\mathbf{P_2W_5}$ is observed, but over time and with the addition of $NaNO_3$, there is a noticeable shift towards more $\mathbf{P_2W_5}$ being formed (Table 4; Supplementary Tables S19, S20). This trend suggests a change in hydrolysis pathways, likely influenced by increased ionic strength.

4 Conclusion

This study, encompassing 648 ^{31}P NMR spectra, investigated the impact of POM concentration, ionic strength, and buffer composition on POM integrity and stability. We observed a general trend of higher POM concentration promoting the stability of the starting compound. Additionally, the composition of hydrolysis products within various buffers was demonstrably influenced by POM concentration. Notably, enhanced hydrolysis or instability was observed at near-neutral pH and with increasing ionic strength.

These findings significantly contribute to the speciation atlas (Gumerova and Rompel, 2023) and as consequence to the field of aquatic POM chemistry. This comprehensive resource catalogs the speciation profiles of common POM archetypes, providing the scientific community with a readily accessible knowledge base of key stability characteristics. This knowledge will be instrumental for future investigations into the biological and catalytic applications of POMs. Furthermore, the study highlights the importance of often-unconsidered experimental parameters on POM behavior in solution, underlining the need for careful consideration of these factors in future POM research.

Data availability statement

The ^{31}P NMR spectra for each condition, replicated in triplicate, are available as raw files in the PHAIDRA repository (https://phaidra.univie.ac.at/o:2069401).

Author contributions

MZ: Data curation, Formal Analysis, Investigation, Visualization, Writing–original draft, Writing–review and editing. NG: Data curation, Formal Analysis, Funding acquisition, Investigation, Methodology, Software, Supervision, Validation, Visualization, Writing–original draft, Writing–review and editing. AR: Conceptualization, Funding acquisition, Project administration, Resources, Supervision, Writing–original draft, Writing–review and editing.

Funding

The author(s) declare that financial support was received for the research, authorship, and/or publication of this article. This research was funded in whole or in part by the Austrian Science Fund (FWF) [DOI 10.55776/P33089 (to AR); DOI 10.55776/P33927 (to NG.)]. For open access purposes, the author has applied a CC BY public copyright license to any author accepted manuscript version arising from this submission.

Acknowledgments

The authors acknowledge ao. Univ.-Prof. Mathea S. Galanski, Ricarda Ofenschüssl, Ing. Susanne Felsinger and Sabine Schneider, NMR Core facility, Faculty of Chemistry, University of Vienna for valuable support during NMR data collection, and ao. Univ.-Prof. Mag. Gerald Giester, Department of Mineralogy and Crystallography, University of Vienna, for cell constants determination of polyoxometalates. The TGA measurements were carried out at the Department of Material Chemistry, Faculty of Chemistry, University of Vienna.

Conflict of interest

The authors declare that the research was conducted in the absence of any commercial or financial relationships that could be construed as a potential conflict of interest.

Publisher's note

Supplementary material

The Supplementary Material for this article can be found online at: https://www.frontiersin.org/articles/10.3389/fchbi.2024.1444359/full#supplementary-material

References

Aureliano, M., Gumerova, N. I., Sciortino, G., Carriba, E., McLauchlan, C. C., Rompel, A., et al. (2021a). Polyoxovanadates with emerging biomedical activities. *Coord. Chem. Rev.* 454, 214144. doi:10.1016/j.ccr.2021.214344

Aureliano, M., Gumerova, N. I., Sciortino, G., Garribba, E., Rompel, A., and Crans, D. C. (2021b). Polyoxovanadates with emerging biomedical activities. *Coord. Chem. Rev.* 447, 214143. doi:10.1016/j.ccr.2021.214143

Bajpe, S. R., Breynaert, E., Robeyns, K., Houthoofd, K., Absillis, G., Mustafa, D., et al. (2012). Chromate-mediated one-step quantitative transformation of PW_{12} into P_2W_{20} polyoxometalates. *Eur. J. Inorg. Chem.* 2012, 3852–3858. doi:10.1002/ejic.201200440

Bijelic, A., Aureliano, M., and Rompel, A. (2018). The antibacterial activity of polyoxometalates: structures, antibiotic effects and future perspectives. *Chem. Commun.* 54, 1153–1169. doi:10.1039/c7cc07549a

Bijelic, A., Aureliano, M., and Rompel, A. (2019). Polyoxometalates as potential next-generation metallodrugs in the combat against cancer. *Angew. Chem. Int. Ed.* 58, 2980–2999. doi:10.1002/anie.201803868

Blasco-Ahicart, M., Soriano-López, J., Carbó, J. J., Poblet, J. M., and Galan-Mascaros, J. R. (2018). Polyoxometalate electrocatalysts based on earth-abundant metals for efficient water oxidation in acidic media. *Nat. Chem.* 10, 24–30. doi:10.1038/nchem.2874

Casas, J., Álvarez, F., and Cifuentes, L. (2000). Aqueous speciation of sulfuric acid–cupric sulfate solutions. *Chem. Eng. Sci.* 55, 6223–6234. doi:10.1016/S0009-2509(00)00421-8

Chaumont, A., and Wipff, G. (2008). Ion aggregation in concentrated aqueous and methanol solutions of polyoxometallates Keggin anions: the effect of counterions investigated by molecular dynamics simulations. *Phys. Chem. Chem. Phys.* 10, 6940–6953. doi:10.1039/b810440a

Collins-Wildman, D. L., Kim, M., Sullivan, K. P., Plonka, A. M., Frenkel, A. I., Musaev, D. G., et al. (2018). Buffer-induced acceleration and inhibition in polyoxometalate-catalyzed organophosphorus ester hydrolysis. *ACS Catal.* 8, 7068–7076. doi:10.1021/acscatal.8b00394

Contant, R. (1987). Relations entre les tungstophosphates apparentés à l'anion $PW_{12}O_{40}^{3-}$. Synthèse et propriétés d'un nouveau polyoxotungstophosphate lacunaire $K_{10}P_2W_{20}O_{70}{\cdot}24H_2O$. *Can. J. Chem.* 65, 568–573. doi:10.1139/v87-100

Faleiro, L., Marques, A., Martins, J., Jordão, L., Nogueira, I., Gumerova, N. I., et al. (2022). The Preyssler-type polyoxotungstate exhibits anti-*quorum* sensing, antibiofilm, and antiviral activities. *Biology* 11, 994. doi:10.3390/biology11070994

Good, N. E., Winget, G. D., Winter, W., Connolly, T. N., Izawa, S., and Singh, R. M. M. (1966). Hydrogen ion buffers for biological research. *Biochemistry* 5, 467–477. doi:10.1021/bi00866a011

Graham, C. R., and Finke, R. G. (2008). The classic Wells–Dawson polyoxometalate, $K_6[\alpha\text{-}P_2W_{18}O_{62}]{\cdot}14H_2O$. Answering an 88 year-old question: what is its preferred, optimum synthesis? *Inorg. Chem.* 47, 3679–3686. doi:10.1021/ic702295y

Gumerova, N. I., and Rompel, A. (2020). Polyoxometalates in solution: speciation under spotlight. *Chem. Soc. Rev.* 49, 7568–7601. doi:10.1039/D0CS00392A

Gumerova, N. I., and Rompel, A. (2021). Interweaving disciplines to advance chemistry: applying polyoxometalates in biology. *Inorg. Chem.* 60, 6109–6114. doi:10.1021/acs.inorgchem.1c00125

Gumerova, N. I., and Rompel, A. (2023). Speciation atlas of polyoxometalates in aqueous solutions. *Sci. Adv.* 9, eadi0814. doi:10.1126/sciadv.adi0814

Harned, H. S. (1958). *The physical chemistry of electrolytic solutions*. New York: Reinhold Pub. Corp.

Keggin, J. F. (1933). Structure of the molecule of 12-phosphotungstic acid. *Nature* 131, 908–909. doi:10.1038/131908b0

Kozhevnikov, I. V. (1998). Catalysis by heteropoly acids and multicomponent polyoxometalates in liquid-phase reactions. *Chem. Rev.* 98, 171–198. doi:10.1021/cr960400y

Lin, B.-Z., Li, Z., Xu, B.-H., He, L.-W., Liu, X.-Z., and Ding, C. (2006). First Strandberg-type polyoxotungstate compound: Synthesis and characterization of organic–inorganic hybrid $(H_2en)(Hen)_2[H_2P_2W_5O_{23}]{\cdot}5.42H_2O$. *J. Mol. Struct.* 825, 87–92. doi:10.1016/j.molstruc.2006.04.027

Machuqueiro, M., and Baptista, A. (2006). Constant-pH molecular dynamics with ionic strength effects: protonation-conformation coupling in decalysine. *J. Phys. Chem. B* 110, 2927–2933. doi:10.1021/JP056456Q

Maksimovskaya, R. I., and Maksimov, G. M. (2019). ^{31}P NMR studies of hydrolytic conversions of 12-tungstophosphoric heteropolyacid. *Coord. Chem. Rev.* 385, 81–99. doi:10.1016/j.ccr.2019.01.014

Massart, R., Contant, R., Fruchart, J. M., Ciabrini, J. P., and Fournier, M. (1977). Phosphorus-31 NMR studies on molybdic and tungstic heteropolyanions. Correlation between structure and chemical shift. *Inorg. Chem.* 16, 2916–2921. doi:10.1021/ic50177a049

Petronek, M. S., Allen, B. G., Luthe, G., and Stolwijk, J. M. (2022). Polyoxometalate nanoparticles as a potential glioblastoma therapeutic *via* lipid-mediated cell death. *Int. J. Mol. Sci.* 23, 8263. doi:10.3390/ijms23158263

Pigga, J., and Liu, T. (2010). Stability of Keplerate polyoxometalate macroanionic assemblies in salt-containing aqueous solutions. *Inorg. Chim. Acta* 363, 4230–4233. doi:10.1016/J.ICA.2010.06.062

Pimpao, C., da Silva, I. V., Mosca, A. F., Pinho, J. O., Gaspar, M. M., Gumerova, N. I., et al. (2020). The Aquaporin-3-inhibiting potential of polyoxotungstates. *Int. J. Mol. Sci.* 21, 2467. doi:10.3390/ijms21072467

Po, H. N., and Senozan, N. M. (2001). The Henderson-Hasselbalch equation: its history and limitations. *J. Chem. Educ.* 78, 1499–1503. doi:10.1021/ed078p1499

Pope, M. T. (1983). *Heteropoly and isopoly oxometalates*. Berlin: Springer-Verlag.

Pope, M. T., and Müller, A. (1991). Polyoxometalate chemistry: an old field with new dimensions in several disciplines. *Angew. Chem. Int. Ed. Engl.* 30, 34–48. doi:10.1002/anie.1991003411002/anie.199100341

Sedlák, M. (1996). The ionic strength dependence of the structure and dynamics of polyelectrolyte solutions as seen by light scattering: The slow mode dilemma. *J. Chem. Phys.* 105, 10123–10133. doi:10.1063/1.472841

Thomas, P., Chandel, S., Mallick, A., Sreejith, S., Ghosh, N., and Roy, S. (2018). Studying the crystallization of polyoxometalates from colloidal softoxometalates. *Cryst. Growth and Des.* 18, 4068–4075. doi:10.1021/ACS.CGD.8B00443

Tourné, C. M., Tourné, G. F., and Weakley, T. J. R. (1986). Triaquahenicosatungstodiphosphate(6–) heteropolyanion, $[P_2W_{21}O_{71}(OH_2)_3]^{6-}$: X-ray crystallographic and ^{183}W nuclear magnetic resonance structural studies. *J. Chem. Soc. Dalton Trans.*, 2237–2242. doi:10.1039/DT9860002237

Wang, J., Tao, Z., Tian, T., Qiu, J., Qian, H., Zha, Z., et al. (2021). Polyoxometalate nanoclusters: a potential preventative and therapeutic drug for inflammatory bowel disease. *Chem. Eng. J.* 416, 129137. doi:10.1016/j.cej.2021.129137

Wang, S.-S., and Yang, G.-Y. (2015). Recent advances in polyoxometalate-catalyzed reactions. *Chem. Rev.* 115, 4893–4962. doi:10.1021/cr500390v

Zhang, G., Keita, B., Craescu, C., Miron, S., de Oliveira, P., and Nadjo, L. (2007). Polyoxometalate binding to human serum albumin: a thermodynamic and spectroscopic approach. *J. Phys. Chem. B* 111, 11253–11259. doi:10.1021/jp072947u

Zhang, H., Li, M., Liu, Z., Zhang, X., and Du, C. (2022). Two Keggin-type polyoxometalates used as adsorbents with high efficiency and selectivity toward antibiotics and heavy metals. *J. Mol. Struct.* 1267, 133604. doi:10.1016/j.molstruc.2022.133604